

**Figure 6.8.** Summary of stress corrosion crack growth rates in various alloys in the Al-Cu alloy system [51].

**6.1.2.8 Corrosion-Affected Fatigue Behavior.** Generally speaking, the term “corrosion fatigue” refers to the combined simultaneous effects of mechanical and environmental action on subcritical crack growth. It is generally accepted that in the operation of aircraft structures, corrosion occurs in between flights and fatigue loading during flights. This distinction is important in establishing a quantitative framework for characterizing, understanding and predicting damage accumulation in aircraft structures. The effect of prior corrosion, primarily pitting damage and the subsequent fatigue behavior (particularly widespread fatigue) has been the subject of recent research [53-56], and a generalized approach to this particular problem is beginning to emerge [57].

A comprehensive example of the effect of prior corrosion on fatigue is found in the work of Sankaran, et al. [58]. In this study, 7075-T6 samples were corroded to various degrees by exposure to cyclic prohesion exposure per ASTM G85 Annex 5 [59], then subject to fatigue cracking under tensile loading. The assumed damage accumulation process is shown schematically in **Figure 6.9**. The experimental results were compared to predictions of fatigue crack growth from the AFGROW software package, the U.S. Air Force fatigue crack growth software [6]. This is a cyclic exposure protocol involving one-hour exposure to a fog generated from a 0.05% sodium chloride plus 0.35% ammonium sulfate solution at ambient temperature. This exposure is thought to produce more realistic pitting damage at more realistic rates than ASTM B117 continuous neutral salt spray exposure.

Prohesion exposure resulted in the formation of a population of discrete pits across polished alloy surfaces, whose depths were characterized by optical microscopy. **Figure 6.10, and 6.11** shows the distribution of pit depths as a function of exposure time. The average pit depth showed a near- $t^{1/3}$  dependence as suggested by the pit growth modeling work of Wei and co-workers for pits in this size range [29]. Pit depths ranged up to about 100  $\mu\text{m}$  in depth. Such pits were capable of initiating fatigue cracks under constant amplitude loading of 414 MPa stress amplitude, R ratio of 0.02 and a frequency of 15 Hz. Notable losses in fatigue life were induced when the average depth of pitting was only 15  $\mu\text{m}$ . Pitting damage reduced fatigue life by a factor of 6 to 8 for an average pitting depth of 50  $\mu\text{m}$ . (**Figure 6.12**). Post test evaluation suggested that pits close to the average size in a particular distribution tended to nucleate the crack leading to ultimate failure rather than the largest pits. This was believed to be due to the fact that there are many more pits of near the average size of the distribution compared to pits at the largest sizes.

This study also showed excellent agreement between the observed fatigue lives and those predicted by AFGROW indicating that this particular model has promise for predicting corrosion-initiated fatigue in high-strength aluminum alloys.

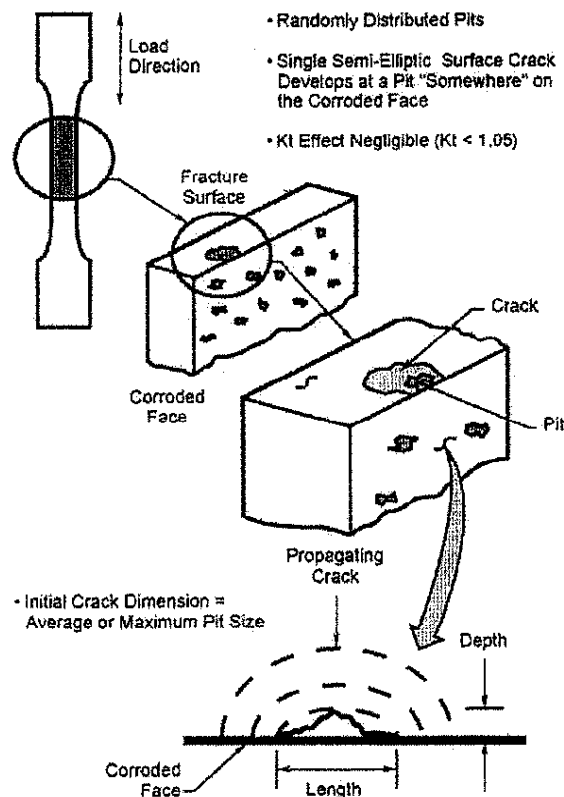


**Figure 6.9.** Schematic illustration of the corrosion-assisted fatigue damage accumulation process and uniaxial testing for resistance to fatigue cracking [58].

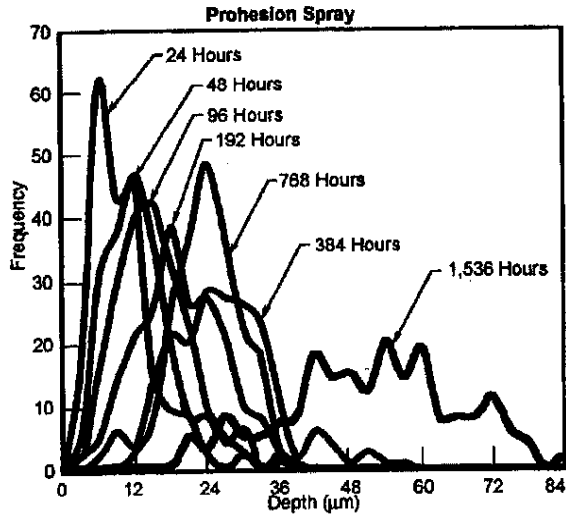


**Figure 6.10.** Pit depth distributions for 7075-T6 from exposure to prohesion spray per ASTM G85 for times indicated in the plot [58].

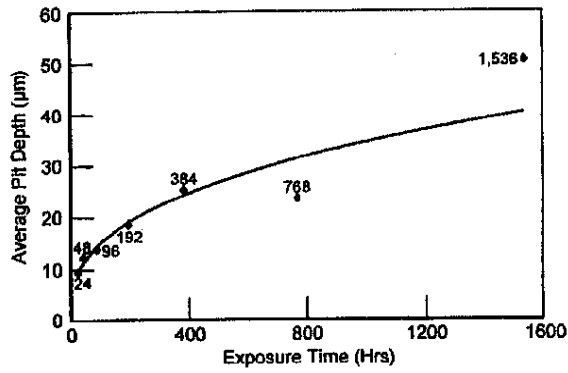


**Figure 6.11.** Average pit depth as a function of prohesion exposure time [58].

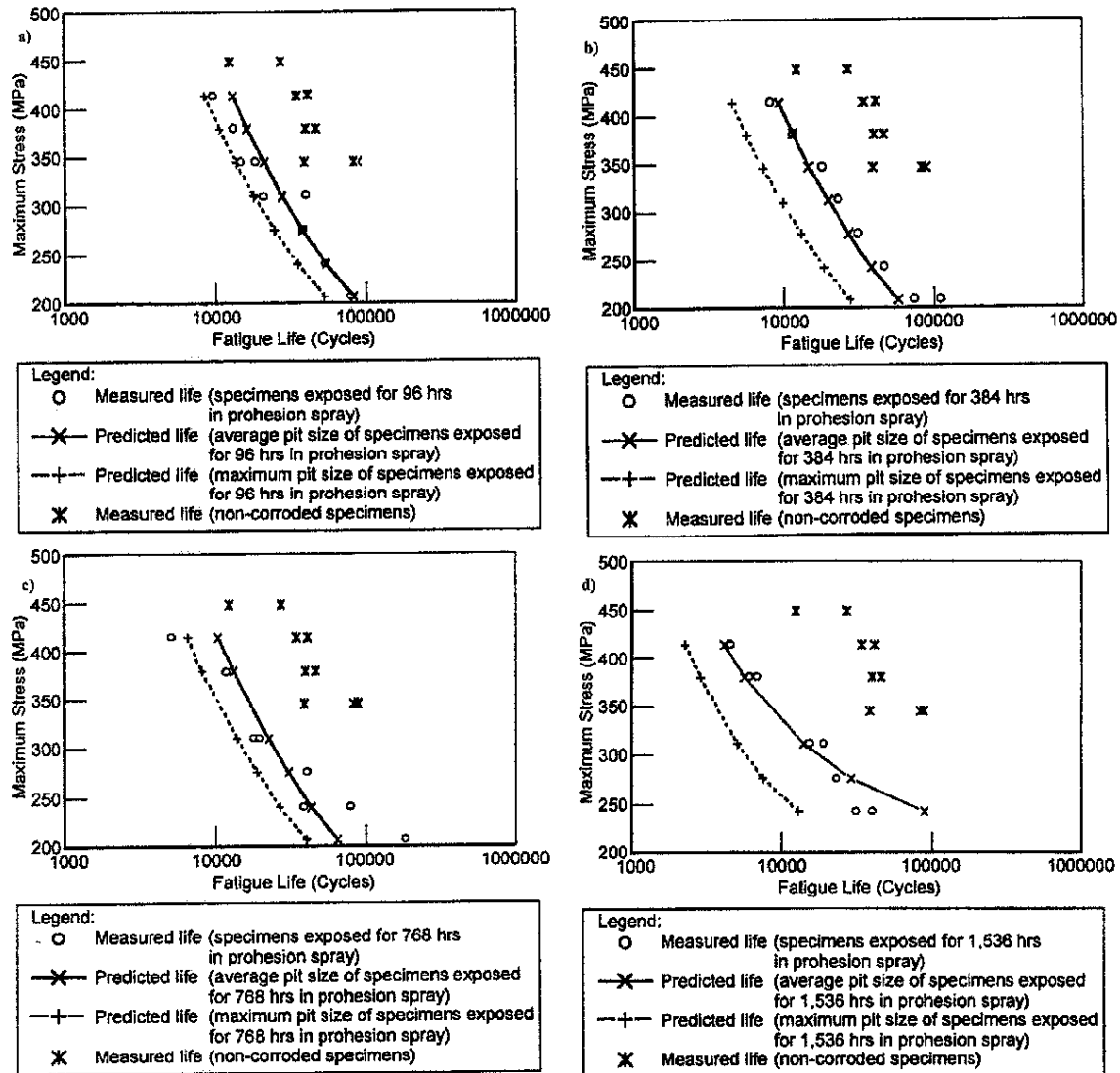


**Figure 6.12.** Predicted and measured fatigue lives for 7075-T6 exposed to prohesion exposure for a) 96 hours, b) 384 hours, c) 768 hours, and 1536 hours [58].

Wei, Harlow and co-workers have approached the problem of corrosion-initiated corrosion fatigue in 2024-T3 and 7075-T6 in a comprehensive fashion by considering quantitatively the onset of localized corrosion damage, the transition from pitting to fatigue crack growth, the early stages of corrosion fatigue crack growth in the short crack regime and fatigue crack growth in the long-crack regime [17, 20, 28, 29, 60, 61]. Their research efforts have focused on 1) the identification of key variables that affect corrosion and fatigue damage recognizing that each component of this damage process is stochastic in nature, 2) the use of probability distribution functions to describe key random variables in mechanistic models, 3) the development of deterministic model frameworks that account for the effect of key random variables on damage accumulation, and 4) integration of models and probability distribution functions to support life prediction and reliability assessments. Strictly speaking, this work considers *corrosion fatigue cracking* triggered by pitting as opposed to the situation where pitting corrosion

precedes and triggers mechanically-driven fatigue crack growth. Nonetheless, this general approach is amenable to corrosion-triggered fatigue and taken together, the elements of this work illustrate a comprehensive approach to the corrosion-assisted fatigue damage accumulation problem.

Elements of the mechanistic corrosion damage accumulation model were presented earlier (**section 6.1.2.3**). Pits transition to corrosion fatigue cracks when the stress intensity factor associated with a pit exceeds the threshold stress intensity for fatigue crack growth:

$$\Delta K \geq \Delta K_{th} \quad (\text{eq. 6.3})$$

and the fatigue crack growth rate exceeds the pit growth rate:

$$\left(\frac{dc}{dt}\right)_{crack} \geq \left(\frac{dc}{dt}\right)_{pit} \quad (\text{eq. 6.4}).$$

Fatigue cracks propagate according to a characteristic power law:

$$\left(\frac{da}{dN}\right)_c = C_c (\Delta K)^{n_c} \quad (\text{eq. 6.5})$$

where  $da/dN$  represents the crack growth increment per load cycle,  $\Delta K$  is the mechanical crack tip driving force and  $C_c$  and  $n_c$  are random variables that represent the contributions of environment and microstructure to the crack growth. **Figure 6.13** schematically illustrates the damage accumulation process represented by this model framework.

This model can be used in at least two important ways [8]. First, by representing random variables in the various mechanistic expressions by empirically-derived Weibull distributions, the dependence of fatigue life to each variable can be determined via Monte Carlo simulation. **Figure 6.14** shows the cumulative distribution functions for the fatigue life of high strength aluminum under fixed loading conditions as a function of the variability in key random variables in the mechanistic expressions that comprise the damage accumulation model. This is essentially a sensitivity analysis that allows the effects of key random variables in the damage accumulation process to be quantified and ranked. Alternatively, full variability of each random variable can be imparted and the effect of changes in an external variable such as stress level can be characterized (**Figure 6.15**).

This model has been benchmarked against field return corrosion data. **Figure 6.16** compares the distribution of observed damage size from a transport aircraft that had been in service for 24 years. These data were compared to model predictions in which the dispersion in the random variables was determined by short term laboratory testing. The

comparison shows that the short term testing data used captured the dispersion in the damage size distribution after 24 years of service with great fidelity.

**Research recommendations for corrosion-affected fatigue.** *Because of the prevalence of this damage mode in airframes, the area of corrosion-affected fatigue growth is the most thoroughly studied and presently the best understood damage accumulation process in high strength Al alloys used in aerospace applications. Comprehensive model frameworks with some mechanistic underpinning have been developed to account for this type of damage accumulation. This understanding should be adapted to the problem of dynamic systems in propeller-driven aircraft to the greatest extent possible.*

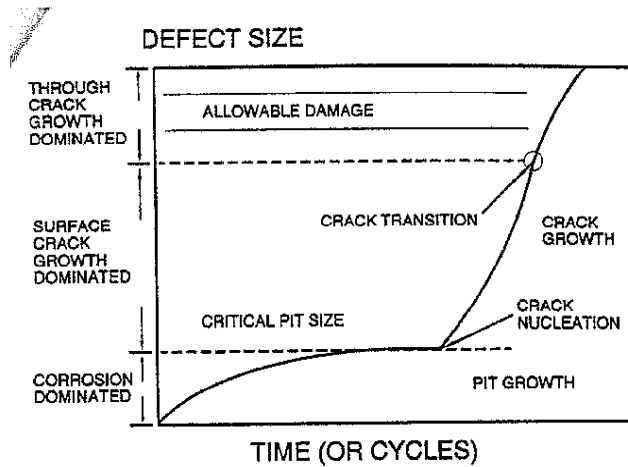


**Figure 6.13.** Schematic representation of pitting corrosion-assisted fatigue crack growth [61].

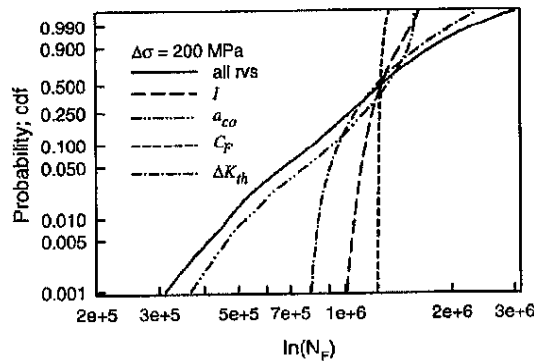


**Figure 6.14.** Simulation of the failure probability showing the sensitivity of fatigue lives to variability in each on the model random variables ( $\Delta\sigma = 200\text{MPa}$ ) [8].

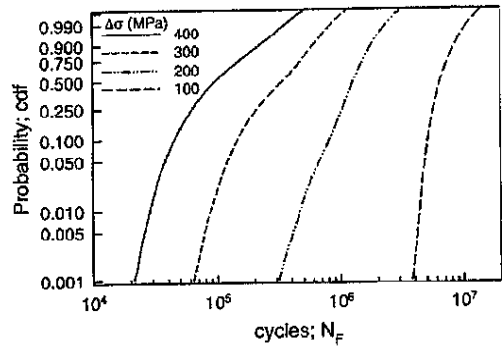


Figure 6.15. Failure probabilities for fatigue life as a function of  $\Delta\sigma$  [8].

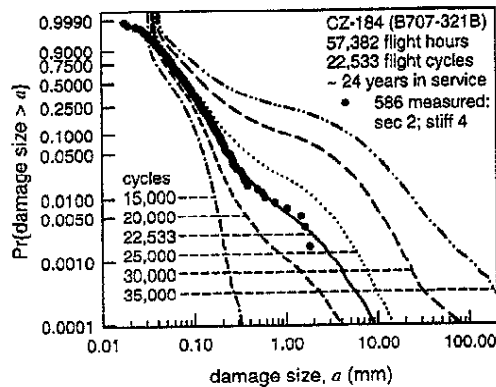


Figure 6.16. Estimated evolution and distribution versus observations from field returns on a 24 year-old transport aircraft [8].

### 6.1.3 Surface finishing for corrosion protection

**6.1.3.1 Cleaning, degreasing and deoxidation.** Standard procedures for surface finishing wrought Al alloys include detergent washing to remove bulk oils, greases and dirt, alkaline degreasing to remove molecular organic contamination and acid deoxidation to remove the original mill-formed oxide scale and to make the surface receptive to subsequently applied conversion coatings.

**6.1.3.2 Conversion Coating.** On aluminum alloys, conversion coatings are essentially artificial passive films whose protective properties exceed those of the naturally formed films. Conversion coatings are typically formed during exposure of a cleaned and deoxidized surface to a specially formulated aqueous solution. Coatings form spontaneously in a matter of seconds or minutes during application by spraying, dipping, immersion or roll-coating. The resulting coatings are usually quite thin, on the order of a few micrometers. They are primarily intended to serve as a base for subsequently applied paints and adhesives. For aluminum alloys, some limited corrosion protection is provided by conversion coatings and they are used for stand-alone corrosion protection when

exposure conditions are expected to be mild (e.g., indoor or enclosed atmospheric exposure).

**6.1.3.3 Chromate-based processes.** Chromate conversion coatings (CCCs) are applied widely on aluminum alloy components on aircraft. Despite the toxicity issues associated with hexavalent chromium, and costs and logistics associated with handling chromate-bearing waste, CCCs continue to be used widely in original manufacture of aircraft components and aircraft refurbishment. In North America, there appears to be little or no momentum behind a shift to chromate-free conversion coating processes. The reasons cited are lack of performance and manufacturability of replacements and the critical need for high levels of corrosion protection for aircraft components and systems. Without a governmental prohibition against the use of chromates in surface finishing, and in the absence of suitable alternatives, it appears that chromate-based processes will be available for some time provided that the metal finishing suppliers continue to support these technologies. In Europe, there appears to be a greater drive to insert Cr-free processes into aircraft systems due to new and expected regulations imposed by the European Union governing use of heavy metals in coatings, but the extent to which this has occurred is still limited.

Chromate surface finishing is mature and trusted. CCC formulations and have been used without significant change since the early 1970s. Nonetheless, during the 1990s there were several large research efforts supported by the DoD dedicated to developing fundamental understanding of chromate corrosion protection including that provided by CCCs. This work is now largely complete and is available in comprehensive reviews [62-64]. The rationale for supporting this work was to develop an understanding of the core functions of chromate protection so that it might be more effectively replicated in emerging Cr-free technology development efforts. This support was motivated by the observation that Cr-free corrosion protection technology, which had been underway with significant industrial and government support, had not delivered a solution to the chromate replacement problem despite 20-plus years of effort. Armed with a better understanding of how chromates protect, it was rationalized that solutions to the problem might be more readily developed.

Modern conversion coating formulations are of two basic types: unaccelerated and accelerated. Unaccelerated baths, such as Alodine 600 and 600H contain a film forming agent—chromic acid and an activator—usually sodium fluoride. Accelerated formulations contain an additive to stimulate film building. In commercial formulations such as Alodine 1200S and Alumigold these additives are ferricyanide or a molybdate compounds. Conversion coating baths are acidic with solution pH values ranging from 1.6 to 1.8. In both accelerated and unaccelerated formulations, the film builds by reduction of  $\text{Cr}^{6+}$  to  $\text{Cr}^{3+}$  followed by hydrolysis, condensation and polymerization of  $\text{Cr}^{3+}$  to form an amorphous  $\text{Cr}(\text{OH})_3$  network (**Figure 6.17**). Under the prevailing acidic bath conditions, unreduced  $\text{Cr}^{6+}$  is bound onto this network as dichromate. Under neutral and mildly alkaline conditions typical of service, dichromate can be released from the backbone leading to the well known self-healing effect demonstrated by CCCs.

Accelerants are specifically added as film thickness builders. They are intended to help attain specified coatings weights in as short a process time as possible. They are believed to work by mediating the  $\text{Cr}^{6+}$  to  $\text{Cr}^{3+}$  reduction reaction, which can be slow on Al and Al alloy surfaces. CCCs produced by accelerated processes are not necessarily more corrosion resistant than those produced by unaccelerated formulations. In fact, it has been reported that preferential adsorption of  $\text{Fe}(\text{CN})_6^{3-}$  on Cu-rich intermetallic particles suppresses the intended film building reactions at those sites perhaps contributing to reduced protection of Al-Cu-based alloys. Among all the high strength aluminum alloys those whose major alloying element is Cu prove to be the most difficult to protect.

Chromate conversion coatings form an inert barrier over the underlying Al substrate. A very strong covalent  $\text{Cr}^{3+}$ -O-Al substrate bond forms the foundation of the coating. This bond is difficult to hydrolyze giving rise to excellent barrier properties and very strong artificial passivity. Dichromate, which is reversibly bound to the  $\text{Cr}(\text{OH})_3$  network can be released into an attacking solution, migrate to coating defects where it is reduced to form a protective  $\text{Cr}^{3+}$ -O-Al substrate bond. This latter phenomenon is often referred to as "self-healing".

Chromate conversion coatings are time and temperature sensitive. Exposure of CCCs to elevated temperatures induces dehydration and further polymerization of the coatings that can lead to an increase in coating cracking, trapping of leachable dichromate and an attendant loss in corrosion protection. Practical guidance indicates that CCCs should not be exposed to temperatures in excess of  $60^\circ\text{C}$ . Coating properties will also change with coating age. These changes are gradual but are also due to dehydration and continued polymerization. Over the span of about a month, losses in self-healing corrosion protection can be detected by electrochemical corrosion testing. Over the span of several years the amount of leachable dichromate is observed to decrease. Over time scales approaching 20 years, the amount of hexavalent chromium in the coating has been observed to diminish significantly. The few measurements that have been made of "old" conversion coatings of this type suggest that coating barrier properties remain largely intact and that good salt spray corrosion performance can be retained.

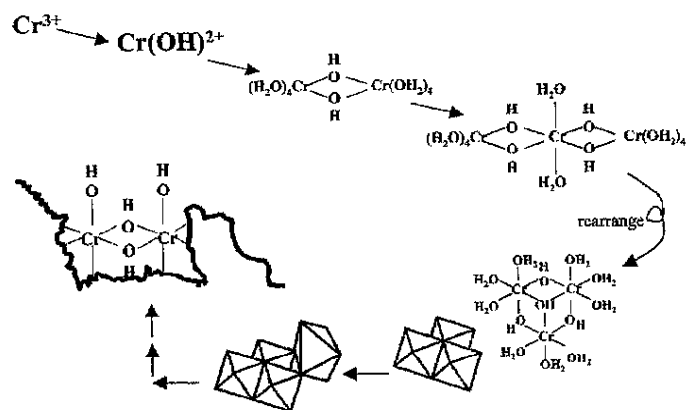


**Figure 6.17.** Schematic illustration of the hydrolysis-polymerization-condensation process that leads to CCC formation [65].

**6.1.3.4 Non-chromate processes.** A plethora of Cr-free surface finishing technologies have been developed and reported over the past 20 years. Many of these coatings have been subject to independent evaluation by trade organizations and by military agencies. The results of these evaluations are available in public reports, which are summarized below. These studies show that a broad range of ad hoc approaches to surface finishing for corrosion protection have begun to organize around a few core strategies that have proven to provide attractive levels of corrosion protection. Nonetheless, these studies also show that no completely Cr-free coating or coating system has yet regularly and repeatably matched the corrosion protection by chromates.

**6.1.3.5 Cr-free conversion coatings and Cr-free, low -VOC coating systems.** Over the past 15 years, there has been considerable effort aimed at developing Cr-free inhibitors and coating systems. Several reviews of the subject exist [63, 66-69]. These reviews show that a very broad range of approaches and chemistries has been considered. Several commercial Cr-free conversion coating technologies [70, 71], and a somewhat greater number of primer coating technologies [72, 73] are available.

In terms of chemistry, the large number of reports and patents related to Ce indicate that it is an excellent inhibitor of metal corrosion [63]. Among non-Cr corrosion inhibitors, the mechanistic understanding of Ce inhibition is clearly the most developed [74]. Other notable transition metal inhibitors are Mn, Co, V, W, Mo, and Fe. These are distinguished by the fact that they can strongly inhibit corrosion under the proper conditions and have been cited in many Cr-free coating patents [63]. This particular

group of inhibitors is also distinguished by the fact that they can exhibit active corrosion protection like chromate coatings.

Sufficient intercoat adhesion is essential for durable coating systems. In recent years, silane coupling agents [75, 76] and functionally graded or tailored sol-gel coatings [77] have been explored for these purposes with some measure of success. These systems derive high adhesion from covalent bonding with the metal substrate and organic topcoats.

**6.1.3.6 Cr-free coating system studies.** Several important surveys of Cr-free coating technology have been undertaken in the past several years. These studies have primarily attempted to survey existing commercial and near-commercial processes to determine if suitable coating systems are possible for demanding military and commercial applications. They have tended to focus more on coating performance determined by test methods prescribed in military specifications and less on the protection mechanisms. The noteworthy result of these studies is that no completely Cr-free coating system has been able to meet stringent corrosion resistance requirements like those established in MIL-P-23377. The following synopses do not represent a comprehensive list of such studies, but are representative of activities conducted in the DOD and industry.

Advanced Corrosion Resistant Aircraft Coatings (ACRAC). The ACRAC program was conducted by a Boeing-led, AFRL-managed team between 1996 and 2000 [78]. The phase-I objective of this program was to adapt existing or emerging coating technologies for Air Force needs in the 2-3 year time frame. The phase-II objective was aimed at "mid-term" needs (5 years), which were defined as improving (decreasing) the environmental impact of coating systems while increasing durability to reduce or eliminate field maintenance and repair. In this program, a coating system was defined as (1) metal cleaning, deoxidizing treatment, (2) conversion coating, (3) primer and (4) topcoat. Performance was evaluated on a system level. In phase-I studies, components examined were limited to commercially available products. Conversion coatings examined include Alodine 1200 and 600 as controls and Bogel EP II, which is a dilute aqueous Zr and Si alkoxide sol-gel system. The silicon component in this system carries an organic group that can be tailored for compatibility with organic topcoats. Chromated primers conforming with MIL-P-23377 (solvent borne) and MIL-PRF-85582 (waterborne) were used as controls. The non-chromated primers tested were Deft 44-W-22, and Dexter Crown Metro 10PW22-2 and US Paint Batch GD99037-38-1, all of which were being developed to meet MIL-PRF-85582 performance requirements at the time. A fluorinated polyurethane supplied by Deft and referred to as the Advanced Performance Coating (APC), was used as the top coat in these studies.

This study led to the important finding that no completely Cr-free coating system tested was capable of meeting the specified 2000-hour neutral salt spray corrosion resistance requirement [78]. Specifically, fully chromated coating systems, and coating systems with a chromated primer exceeded 2500 hours of exposure. A coating system with a chromate-free primer and a chromate conversion coating demonstrated about 2000

hours of salt spray resistance, but a completely chromate-free system exhibited only about 1200 hours before significant corrosion occurred.

The second phase of the study was aimed at developing hybrid coatings that would replace both the conversion coating and the primer coating. Several different approaches were explored based generally on integration of sol-gel, epoxy and inhibitor components. Inhibitors based on Ce, V, B, and thiol compounds were down-selected for study within this development effort as a result of a larger survey of inhibitor efficacy [79]. This study did not develop a successful hybrid replacement and highlighted the need for serious pigment development research for corrosion resistant primer applications.

The NCMS Chromium Alternatives study. This study was conducted from 1993 to 1995 by a task group representing industry, academia, and federal labs [70]. The project was organized and carried out under the auspices of the National Center for Manufacturing Sciences (NCMS). The intent was to survey the state of the art with respect to chromate-free conversion coatings. A set of 29 commercial and pre-commercial Cr-free conversion coatings, obtained from 12 different vendors, were applied to 5 different alloy substrate types. The corrosion resistance, paint adhesion and electrical contact resistance of Cr-free samples, and chromated control samples were evaluated and reported. An environmental impact assessment of the various Cr-free coating processes was also conducted. The significant finding from this study was that none of the Cr-free alternative coatings was able to meet the performance requirements for conversion coatings established in MIL-C-5541E or MIL-C-81706. Accordingly, no Cr-free conversion coating system appeared suitable for demanding military applications. A new NCMS survey of Cr-free conversion coating technology was completed in 2001 [80].

Joint Group on Pollution Prevention (JG-PP). JG-PP is charged with addressing issues related to reduction in use of hazardous materials across the various branches of the military, NASA and the Defense Contracting Management Agency. Several technology evaluations relevant to high performance coating systems have been conducted under the auspices of JG-PP, including surveys of conversion coatings [71], Cr-free primers [72], and Cr-free coating systems [73]. The common approach in these evaluations is to identify commercial technologies and evaluate on the basis of service-mandated performance testing, and environment safety and health concerns. These tests have shown that there are promising conversion coating and primer coating technologies available, but no completely Cr-free coating system achieves the MIL-P-23377 corrosion resistance requirement.

***Research recommendations on coatings:*** *Prospects for the introduction of new materials and process into dynamic systems is possibly greatest in the area of surface treatments and coatings. Because strict corrosion prevention is essential in dynamic system components it is essential that new materials and processes be introduced according to strict performance requirements, and with a quantitative understanding of their effect on localized corrosion initiation, differentiation and propagation. Because small amounts of corrosion damage can significantly impact safety, commonly used qualification approaches for new coatings and coating systems may not be sufficiently stringent.*

*Efforts should be made to understand quantitatively how current coating systems prevent corrosion and how long they provide suppression. Additionally, efforts should be made to develop standard methods for determining what corrosion suppression means and how it should be evaluated. Emerging coating systems with high performance should be evaluated against criteria developed.*

## 6.2 Ultrahigh Strength Steels D6ac and AISI 4340

**6.2.1 Physical Metallurgy and Mechanical Properties [81]** . AISI 4340 and D6ac are forgeable medium-carbon low-alloy ultrahigh strength steels. Composition ranges for these alloys are given in **Table 6.4**, and representative mechanical properties are shown in **Table 6.5**. AISI 4340 is the benchmark alloy among ultrahigh strength steels because of its deep hardenability, high ductility and toughness, high strength. It also possesses excellent fatigue and creep resistance. At strengths greater than about 1400 to 1500 MPa, 4340 is susceptible to stress corrosion cracking and hydrogen embrittlement [82]. Generally, alloy steels possess somewhat greater corrosion resistance than carbon steels, though potent corrosion protection is still needed for long-term use in natural environments.

D6ac is an ultrahigh strength steel designed specifically for aerospace and military applications. It is alloyed with vanadium to promote grain refinement. It possesses slightly higher carbon, chromium and molybdenum contents, and a lower nickel content than 4340. D6ac is also distinguished by its production method. The alloy is produced in an electric furnace by air melting and then vacuum arc remelted. D6ac can be strengthened to a greater degree than 4340 and it demonstrates excellent notch toughness and impact loading resistance. Like 4340, this alloy is susceptible to stress corrosion cracking and hydrogen embrittlement [83]. Crack paths tend to be intergranular following prior austenite grain boundaries and the extent of carbide precipitation along these boundaries may be an important controlling factor. Resistance to fatigue cracking is strongly environment sensitive. The fatigue life in water saturated air is 35% of that in very dry air [84].

In aircraft and aerospace applications the primary failure modes for 4340 and D6ac are pitting, fatigue and corrosion fatigue initiated from pits, hydrogen-induced cracking and stress corrosion cracking.

**Table 6.4.** Composition limits for 4340 and D6ac

Alloy	C	Mn	Si	Cr	Ni	Mo	V
4340	0.38 – 0.40	0.60-0.80	0.20-0.35	0.70-0.90	1.65-2.00	0.20-0.30	
D6ac	0.42-0.48	0.60-0.90	0.15-0.30	0.90-1.20	0.40-0.70	0.90-1.10	0.05-0.10

**Table 6.5.** Representative mechanical properties for 4340 and D6ac

Alloy	Tensile Strength (MPa)	Yield Strength (MPa)	Elongation (%)	Charpy Impact Energy (J)	Fatigue Limit (MPa)	KIC (MPa)	KISCC (MPa)
4340 <sup>a</sup>	1980	1860	11.0	20	540	53	8 <sup>†</sup>
D6ac <sup>b</sup>	2060	1450	8.5	14	760		

a- oil quenched from 845°C and tempered at 205°C.

b-normalized at 900°C, oil quenched from 845°C, tempered at 150°C.

† in seawater.

Steels of this type derive their properties from hardening heat treatments and tempering. Normalization or annealing heat treatments are used to homogenize the alloy microstructure. Austenitizing heat treatments develop a predominantly or fully austenitic structure in the material. Careful quenching from the austenitizing temperature allows the formation of lower bainite and martensite, which contribute significantly to the desirable mix of properties developed in the alloys. Tempering and spheroidizing are used to relieve residual stresses, impart improved plasticity and toughness. These gains are accompanied by a loss in strength. Heat treatment results in a mixed martensitic-bainitic structure. Additions of Cr, V and Mo lead to a dispersion of carbides that contribute to strength and toughness. A representative TEM micrograph of the tempered martensite structure of D6ac is shown in **Figure 6.18**.



**Figure 6.18.** TEM micrographs of D6ac austenitized at 872°C for 40 minutes, cooled to room temperature under flowing nitrogen tempered at 300°C for 2 hours showing nearly continuous carbide precipitation along prior austenite grain boundaries [83].

## 6.2.2 Corrosion Behavior

**6.2.2.1 Pitting.** The pitting behavior of high strength alloy steels is very well characterized [85]. Pitting in these materials generally initiates at inclusions in the alloy, such as MnS particles. Pits tend to be hemispherical initially, but then grow in breadth more than they do in depth. Mature pits take on an irregular morphology and may link up forming large pit clusters. Tensile stress in the plane of the pitting surface may lead to the formation of sharp pits, or sharp protrusions from the base of pits.

Alloy steels are prone to pitting in a range of environments, pit growth is affected by the chemical aggressiveness of the environment, temperature and pH [86].

In early stages, pit growth (depth) is reported to depend approximately on the cube root of time [87] :

$$d = At^{1/3} \quad (\text{eq. 6.6}).$$

The constant A has been shown to depend on environmental conditions and stress [88]. The growth rate has been expressed in terms of the pit dissolution rate using Faraday' law [89]:

$$d = \left( \frac{3Mit}{2\pi zF\rho} \right)^{1/3} \quad (\text{eq. 6.7})$$

where M is equivalent atomic weight, I is the pit current, t is time, z is the oxidation state of the dissolved metal, F is Faraday's constant (96500 C/eq), and  $\rho$  is density. From a range of experiments, the value of the exponent that characterizes the time dependence is not strongly dependent on environment and applied mechanical stress, but in some cases is found to be somewhat less than 1/3 [88], and somewhat greater than 1/3 in others [90] perhaps reflecting the fact that pits deviate from hemispherical shape as they grow. Pit growth laws, such as the one shown in eq. 6.7 have been used successfully to predict the evolution of a distributions of pits growing in alloy steels.

Empirical modeling approaches based on measurement and fitting of pit depth data have also been carried out successfully. Pit depths distributions are well characterized by a three-parameter Weibull function. The time-dependence in the shape, scale and location parameters has been determined from fitting of pit depth distributions as a function of exposure time to make empirically-based models for predicting pit growth. Models such as these have been incorporated into models for predicting stress corrosion and fatigue crack growth from pits and are discussed below.

One area in which there is not good understanding is in the area of pit initiation. Some methodologies for characterizing pit initiation tendencies as a function of metallurgical, environmental and surface condition variables have been developed using stainless steels [91]. These results are not directly applicable to pitting corrosion in alloy

steels, but the methodologies and analyses are readily adaptable and could be extended to understand the effects of coatings on pit initiation.

With the exception of the problem of initiation, pitting corrosion in high strength alloy steels has been well characterized. Empirical and semi-mechanistic models have been developed and used to predict the evolution of pitting damage. This understanding and modeling is readily adaptable for application to aircraft propeller corrosion problems. Pit initiation has been characterized using a statistical perspective. Pit growth models are well established for predicting the evolution of pit depth and shape.

**Research recommendation pitting of steels.** *Good characterizations of the pitting of alloy steels in aqueous environments have been reported in the literature. From these data and from selected experiments, efforts should be made to develop and validate a predictive model. Efforts should also be made to integrate such a model or models to larger frameworks for predicting the accumulation of other forms of corrosion such as fatigue and stress corrosion cracking.*

**6.2.2.2 Stress corrosion cracking.** Ultrahigh strength steels are susceptible to stress corrosion cracking. **Figure 6.19** shows that in distilled water both 4340 and D6ac exhibit well articulated applied stress intensity thresholds below which stress corrosion cracking is not observed. In chloride environments, stress corrosion cracks are observed to initiate from pitting damage. Cracks can follow intergranular or transgranular paths, though the incidence of intergranular fracture tends to be greater. Intergranular SCC follow prior austenite grain boundaries. Unfortunately the fractographic characteristics of SCC, hydrogen embrittlement and temper embrittlement are rather similar [92]. Hence fractography is not always a good means for unequivocally distinguishing the origins of environmentally assisted cracking.

Stress corrosion cracking can occur in chemically mild environments at stresses well below the macroscopic yield strength. In particularly mild environments, SCC may initiate from intergranular corrosion without obvious pitting or corrosion product formation.

The most significant metallurgical characteristic that influences SCC susceptibility is alloy strength level [93]. Increasing alloy strength generally increases SCC susceptibility resulting in classic engineering property trade-off decisions. Increasing alloy strength will decrease  $K_{ISCC}$  as shown in **Figure 6.20**. **Figure 6.21** shows that for equal applied stress intensities, crack growth rates increase substantially as alloy strength is increased. These factors combine to produce an overall decrease the time to failure during exposure to aqueous solutions (**Figure 6.22**). These general trends apply to 4340 as well as D6ac.

Alloy microstructure also plays a strong role in SCC behavior [93]. **Figure 6.23** shows crack velocity versus applied stress intensity curves for 4340 steels in 3.5 % NaCl solution and distilled water processed to form tempered martensite or tempered lower bainite microstructures. The figure shows that SCC crack growth rates are strongly

reduced and  $K_{ISCC}$  increased for bainitic microstructures in both environments tested. This difference has been attributed to more effective trapping of hydrogen at interfaces in the martensite which facilitates SCC. In D6ac, ausforming thermal-mechanical processing to refine the alloy microstructure confers increased cracking resistance as shown in **Figure 6.24**. Such treatments refine the martensite platelet size and homogenize the carbide particle dispersion leading to increases in time to failure during exposure to aqueous environments.

An interesting and potentially important affect on SCC susceptibility is due to the effect of prior creep strain [82]. SCC of ultrahigh strength steels is interpreted in the context of the film-rupture mechanism [94]. According to this mechanism the accumulation of strain from creep of the underlying metal serves to periodically rupture the oxide film at the tip of a stress corrosion crack. Once ruptured, the crack advances by electrochemical dissolution until it repassivates. Experimental result show that when a high strength steel is subject to a period of prior creep in an inert environment, SCC initiation can be delayed or prevented and SC crack growth rates can be retarded.

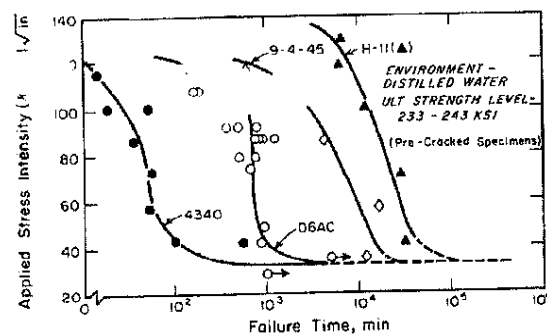


**Figure 6.19.** The effect of stress intensity on time to failure for 4340 in distilled water [93].

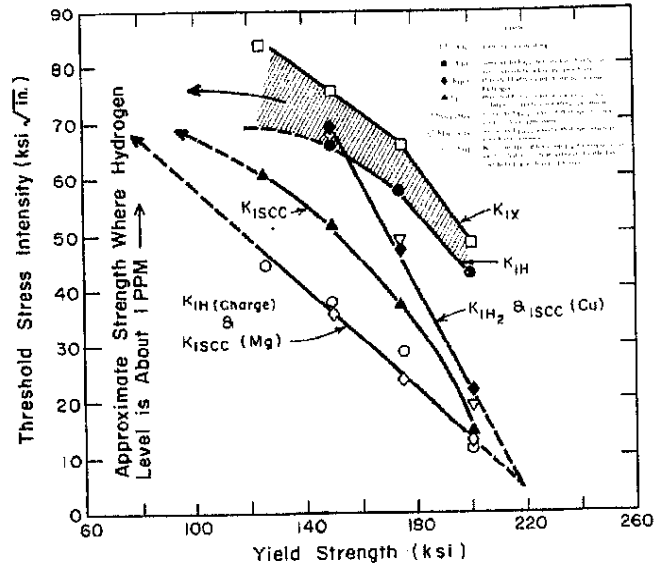


**Figure 6.20.** The effect of yield strength on the threshold stress intensity,  $K_{I,SCC}$ , in 4340 in an aqueous environment [93].

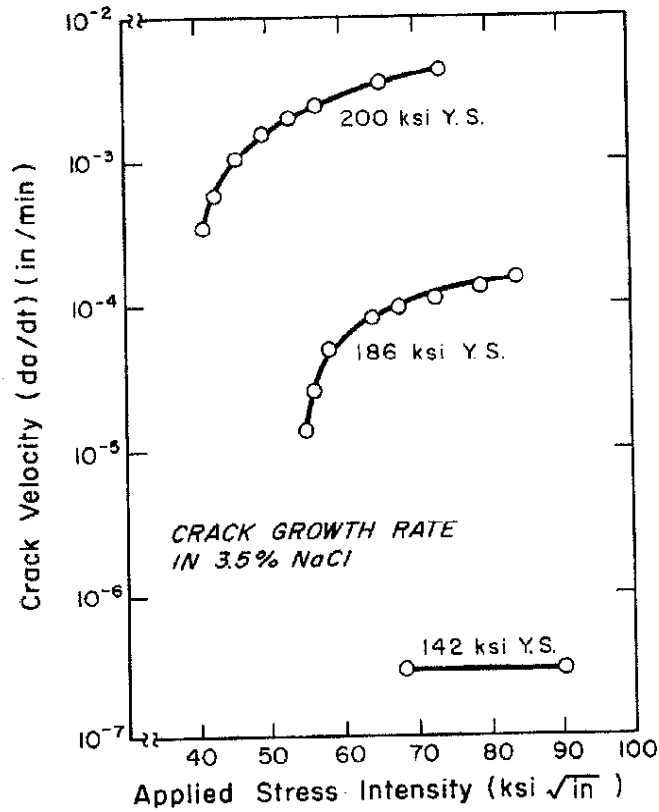


**Figure 6.21.** The effect of applied stress intensity on the crack velocity of 4340 [93].

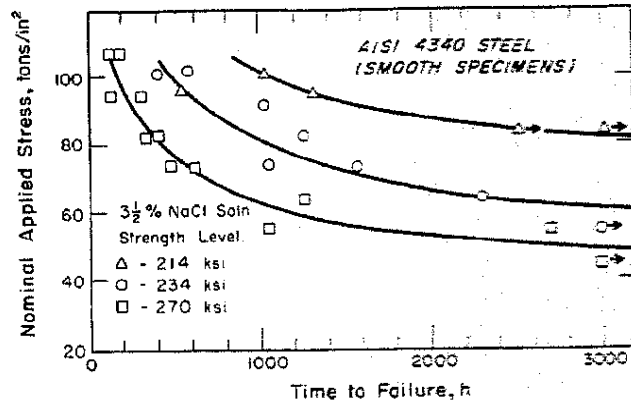


**Figure 6.22.** The effect of strength level on the time to failure of 4340 in 3.5% NaCl solution [93].

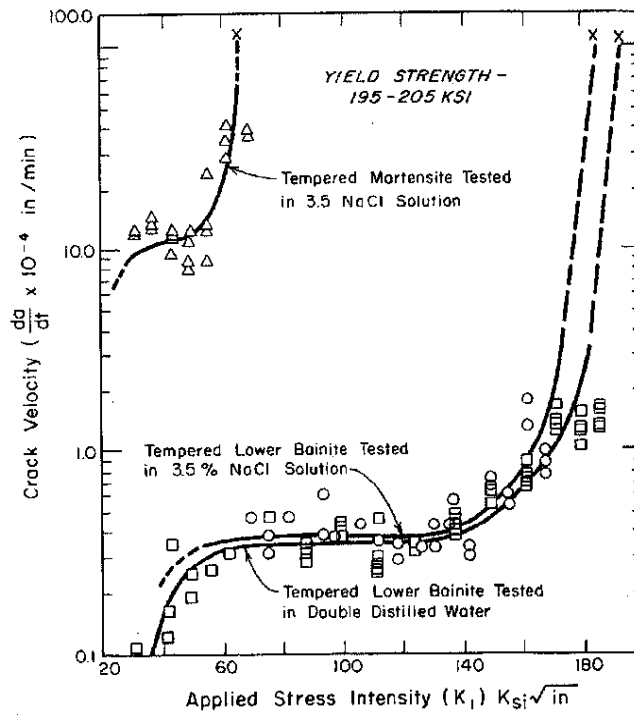


**Figure 6.23.** Crack velocity versus stress intensity for 4340 in 3.5% NaCl solution and distilled water [93].

#### Ausformed

1. Austenitized at 1650 F in air for 2 hours
2. Air cooled to 1050 F, held at 1000 F for ½ hour
3. Reduced 65% by press forging
4. Oil quenched
5. Stress relieved at 350 F for 2 hours
6. Specimens cut out and finish ground
7. Tempered for 2 + 2 hours

#### Conventional

1. Austenitized at 2000 F in air for 1 hour
2. Reduced 65% by press forging
3. Air cooled
4. Specimens cut out and machined 0.025 inch oversize
5. Austenitized at 1650 F in air for 2 hours
6. Oil quenched
7. Stress relieved at 350 F for 2 hours
8. Specimens finish machined to size
9. Tempered for 2 + 2 hours

#### Aus-bay

1. Steps 1 through 8 of conventional treatment
2. Austenitized at 1650 F in salt for 1 hour
3. Transferred rapidly to 950 F salt bath
4. Held in 950 F salt for 5 minutes
5. Quenched in 150 F oil
6. Tempered for 2 + 2 hours

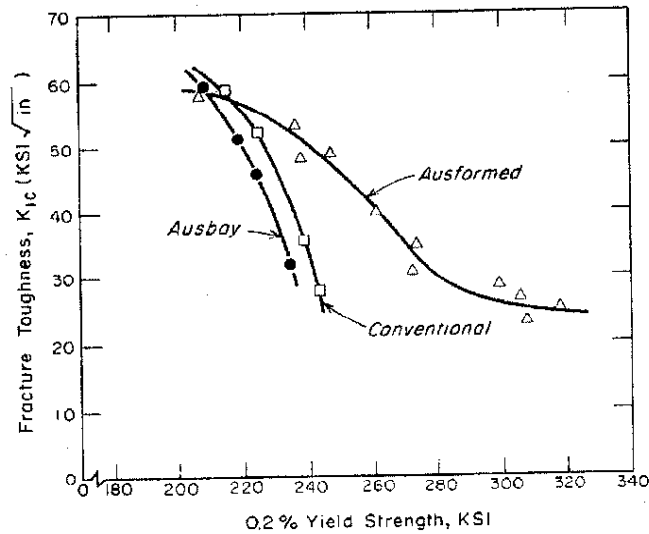


**Figure 6.24.** Effect of thermal-mechanical processing on fracture toughness of D6ac steel [93].

**6.2.2.3 Hydrogen Embrittlement.** Generally speaking, hydrogen embrittlement refers to an immediate loss in ductility and fracture or delayed fracture due to subcritical crack growth under sustained stress [95]. D6ac and 4340 are both susceptible to hydrogen

embrittlement. Hydrogen need not be present at or above the saturation concentration for cracking to become a problem. At low concentrations, evidence for HE is difficult to detect and establishing the details of the degrading hydrogen interaction with the microstructure and difficult to pin down. Generally, susceptibility increases as alloy strength increases. As strength increases local accumulation of hydrogen can be damaging and the total hydrogen content in the alloy may not be a good predictor of susceptibility. Cracking often proceeds along prior austenite grain boundaries. It has been noted that hydrogen embrittlement susceptibility decreases as the coverage of carbides increases. Fractional coverage of carbides can be increased by increasing the tempering temperature. The use of increased tempering temperature also decreases alloy strength. The relative contributions of these parallel effects; grain boundary microstructure and decreased strength on HE susceptibility, have not yet been well separated.

In a vast majority of cases examined, the source of hydrogen in hydrogen-induced failures of D6ac and 4340 has been traced to residual hydrogen from plating operations. The forensic evidence suggests that the opportunity to introduce hydrogen into alloys during service is much smaller than that associated with plating operations. The need for careful degassing heat treatments after plating is thoroughly appreciated and the use of rigorous procedures for carrying out such treatments are standard [92]. Because of the drive for the implementation of higher strength steels in design, alloys can become susceptible to cracking at lower hydrogen contents. This places greater burden on degassing, particularly where thicker section components are to be used.

***Research recommendation for SCC and HE of ultrahigh strength steels.***

*Environmentally assisted crack (EAC) growth rates are very high for high strength steels and it is unlikely that subcritical cracking would be detected between the time of initiation and the attainment of a critical flaw size. However, because the metallurgical and environmental factors contributing to EAC are well established for these materials, consideration should be given to using risk or reliability-based approach for characterizing the possibility of EAC based on manufacturing, properties, corrosion protection schemes used and component age.*

**6.2.2.4 Corrosion Affected Fatigue Behavior.** The influence of prior pitting on fatigue crack initiation and growth is handled for ultrahigh strength steels in much the same manner as that described earlier for aluminum alloys [96]. The general mechanistic and modeling frameworks apply equally well to both steels and aluminum alloys. In actual fact, essential elements of the model for fatigue crack initiation from pits described for aluminum alloys were adapted from models originally developed to address the problem in steels.

The reader is referred to sections 6.1.2.8, Corrosion-affected Fatigue Behavior for Al Alloys, and 6.2.2.1, Pitting of Ultrahigh Strength Steels, and the research recommendations following those sections.

### 6.2.3 Surface finishing for corrosion protection

**6.2.3.1 Cleaning, deoxidation and passivation.** Steels develop oxides scales during hot-working, annealing, or welding that lower corrosion resistance or paint adhesion, and negatively affect fatigue life. Scales are removed using chemical means, mechanical means, or combinations of both. Within the trade, chemical decaling is often referred to as "pickling". In the case of stainless and semi-stainless alloys, additional chemical treatments, commonly referred to as "passivation" processes, are used to ensure maximum resistance to pitting and crevice corrosion by enriching the adherent oxide film with Cr [97], and preferentially dissolving inclusions that serve as pit initiators [98].

Pickling of alloy steels is usually carried out in sulfuric acid solutions ranging in concentration from 3 to 40%, depending on the alloy type and product form [99, 100]. Baths are operated at 60° to 100°C and processing times ranging from tens of seconds to 30 minutes or more. Contact times greater than 30 minutes are not common as the risk for surface etching increases. Steel rod and wire are often pickled using a 1 to 20s immersion in hot hydrochloric acid solutions with concentrations of 6 to 15% by weight at temperatures of 75° to 95°C, or chloride additions to sulfuric acid baths are sometimes used to accelerate the descaling action [101]. Other acid cleaning treatments are used to remove not only oxide scale, but dirt, oils and other contaminants from the steel surface. The use of mineral acids such as phosphoric acid are common in this regard [102]. For structures too large for treatment by immersion, pickling pastes have been developed [103].

**6.2.3.2 Cadmium Plating and Cadmium Replacements.** Cadmium plating was widely used on aircraft components; mainly fasteners and electrical components, to enhance corrosion resistance and promote lubricity on components that are removed and reinserted on a regular basis. The human toxicity of cadmium is well known and has forced elimination of its use in many applications. Aluminum and zinc-based coatings offer attractive mixes of properties and are alternatives to cadmium plating for certain applications [104]. Electrodeposited zinc coatings are formed with the co-deposition of hydrogen and careful post-coating degassing procedures must be followed with for high strength steel substrates. Ion vapor deposition of aluminum coatings is now an industrial process by which pure Al and Al-Mn coatings are formed on a range of substrates.

Alternative coating deposition methods include those based on physical vapor deposition (PVD), chemical vapor deposition (CVD), sputter deposition, or thermal spraying [105]. Al-based coatings can be quite reactive and are sometimes conversion coated to enhance their environmental resistance.

For new coatings applied to ultrahigh strength steel substrates, performance issues beyond corrosion protection include impact on fatigue behavior and hydrogen uptake during or after processing.

**6.2.3.3 Chromium plating and chromium replacements [106].** Chromium plating has been a very widely used surface treatment in the aerospace industry for imparting high

levels of hardness, wear and corrosion resistance. Hexavalent chromium is a potent carcinogen and there has been significant regulatory pressure that has reduced the usage of chrome plating over the past several years.

While chrome plating imparts many desirable characteristics to metal surfaces, it forms with residual tensile stresses. These stresses are partially relieved by the formation of cracks in the plated layer, but still, electroplated Cr layers can reduce the fatigue resistance of high strength steel substrates. Shot peening can relieve surface tensile stresses to some extent.

Alternatives to chromate plating include thermal spray coatings such as tungsten carbide [107], tungsten carbide-cobalt [108], nitride coatings such as titanium nitride [109], and complex carbide-particle transition metal compositions [110]. Corrosion resistance, wear resistance, and fatigue crack growth behavior are all important properties that are typically reported. The performance of thermally sprayed coatings is quite variable and depends on coating chemistry, deposition parameters and coating thickness. At their best, these coatings can offer attractive mixes of properties, however there appears to be a great deal of variability in the characteristics of these coatings at the present time.

**6.2.4 Mechanical surface treatment.** Introduction of compressive surface residual stresses on load bearing components has been shown to reduce susceptibility to stress corrosion cracking and corrosion fatigue. Shot peening is carried out through the controlled bombardment of a metal surface with small hard particles such as steel shot. This surface compressive stress counteract tensile stresses that contribute to various forms of cracking. Shot peened layers are typically 100 to 500  $\mu\text{m}$  in thickness. The beneficial effects of shot peening are lost by elevated temperature treatment or by localized or uniform corrosion to depths that exceed the thickness of the layer.

Newer approaches for producing surface layers in compression are based the use of special tools for carrying out a burnishing-like process [111]. Compressive stresses approaching those developed by shot peening can be induced in layers whose thicknesses match shot peened layer thicknesses. These new technique are still in the development and evaluation stage for aerospace components.

*Research recommendation. See research recommendation for coatings for Al alloys.*

## **7.0 Non-Destructive Evaluation (NDE)**

### **7.1 Overview of NDE.**

In 1990, the Inspection Systems Initiative was established by the FAA to develop and validate airplane inspection technology [112]. The objectives of this initiative were to validate existing and emerging inspection systems with respect to their ability to reliably detect cracks, disbands corrosion and other types of damage

Within the area of dynamic systems in propeller-driven aircraft there is the need for quality assurance in manufactured components and systems and in-service inspection of dynamic and static components.

The standard by which the adequacy of inspection strategies are judged is their probability of detection (PoD) of flaws of specific sizes. PoDs vary depending on flaw size and type, material, component configuration and accessibility, and surface finish. Currently, under best-case conditions for the most sensitive techniques the PoD for cracks is 50% at 1.27 mm. The discussion of corrosion of Al-Cu-Mn and ultrahigh strength steels shows that important parts of the localized corrosion damage accumulation process occur from 0.01 to 0.25 mm size range.

## **7.2 Established methods and detection limits**

**7.2.1 Visual inspection.** Visual inspection is the primary means of corrosion detection for general aviation aircraft. Visual inspection of corrosion is rapid and simple, though care is required to inspect for corrosion in difficult-to-access locations. The primary drawback of visual inspection is that it is possible to miss many forms of localized corrosion, particularly in their earliest stages because they occur without the development of appreciable corrosion product.

**7.2.2 Eddy current.** Eddy current methods are based on the use of probe containing an AC electrical coil that produces a magnetic field, which penetrates the surface to be inspected. If the specimen is a conductor, currents will be induced in the sample and an opposing magnetic field will be generated that in turn decreases the magnetic flux through the coil causing a change in the coil impedance. This impedance change can be detected and used as the basis of the eddy current measurement. Physically small eddy current probes can detect surface breaking cracks as small as 1 mm under ideal circumstances.

**7.2.3 Ultrasonic inspection.** Ultrasonic methods employ a piezoelectric material to inject ultrasonic energy into a material of interest. The waves propagate through the solid and are reflected and scattered by internal surfaces and defects, which can be detected by a properly placed receiving piezo detector. A schematic of a the commonly used pulse-echo detection scheme is shown in **Figure 7.1**. In this arrangement, the detector injects a pulse of ultrasonic energy at some prescribed frequency and the listens for the returns from reflections of internal surfaces and the back surface. By analyzing the time and intensity of the returns, the defect location and size can be estimated. The sensitivity of ultrasonic measurements to defects is dependent on a wide range of variables including skill of the analyst, but detection of crack and corrosion-like defects less than 0.5 mm in size in complex component structures is extremely challenging.

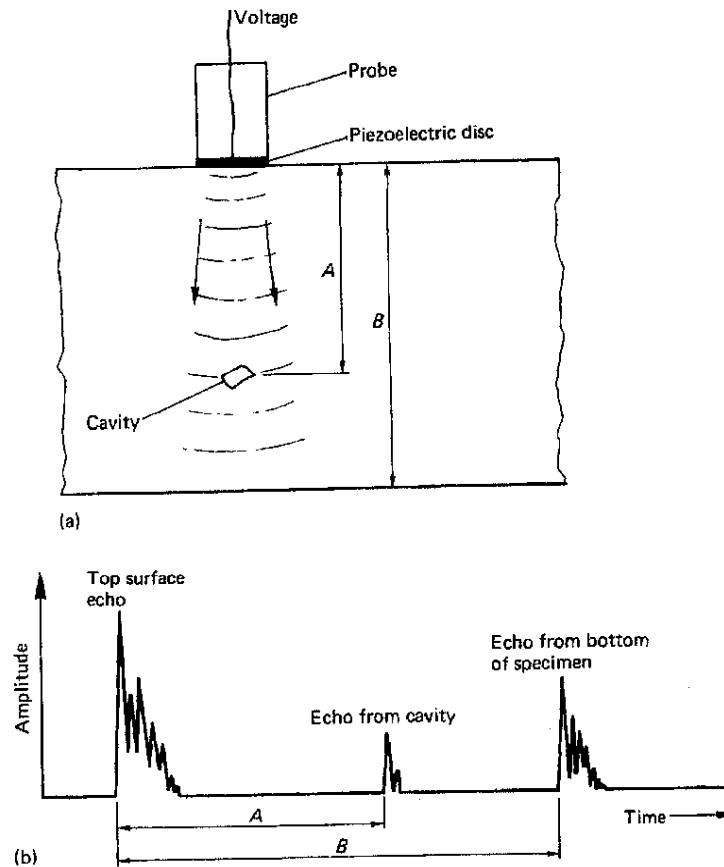


Figure 7.1. Pulse-echo detection in ultrasonic testing [113].

**7.2.4 X-ray Radiography.** X-ray radiography (radiography) is based on the fact that x- and gamma-radiation can penetrate solids with partial absorption during transmission. The extent of transmission is determined by the transmission path length and the absorption characteristics of the material. Radiography is well suited for revealing volumetric defects such as inclusions, voids, porosity, and surface thinning. Large cracks can also be detected depending on the geometry with which they are viewed. Small cracks that present little volume are difficult or impossible to detect. Radiography can be used to check the presence of voids and inclusions in forging stock used in manufacturing propeller components. It is not well suited for detecting small cracks under 0.5mm in length.

An exception to this general limitation is found in an adaptation of the radiographic technique called microfocal radiography. Microfocal radiography uses a bright, geometrically small monochromatic x-ray source and projection magnification to resolve corrosion defects at micrometer length scales [114]. Phase contrast techniques have been employed to further enhance resolution and information content of radiographic images.

**7.2.5 Liquid penetrant dye inspection.** Liquid penetrant techniques are among the oldest non-destructive techniques available, and are well suited for detection of surface-

breaking cracks on boldly exposed surfaces. The method involves applying a penetrating liquid to a cleaned surface, removing the excess fluid, then applying a “developer” to aid in revealing any fluid that emerges from small surface breaking cracks or pits. A wide range of penetrants and developers are commercially available and sensitivity of the technique can be enhanced by the use of penetrant dyes that fluoresce under UV light. These approaches may be sensitive to micrometer-sized pits and cracks, but extracting unequivocal defect indications on surfaces with micrometer-level surface roughness is extremely difficult.

### **7.3 Emerging methods.**

#### **7.3.1 Superconducting quantum interference device (SQUID) magnetometry.**

SQUID magnetometry uses a cryogenically cooled magnetometer to detect changes in magnetic flux with great sensitivity in electrical conducting and ferromagnetic materials [115]. SQUID magnetometers are sensitive to magnetic anomalies associated with electric current. A class of NDE approaches based on the induction of eddy currents and detection of magnetic anomalies due to defects in sample have been derived from this method [116]. SQUID magnetometers have also been adapted to sense changes in magnetic fields due to corrosion currents from actively corroding components [117]. Because SQUID detectors operated at some standoff distance, they are able to detect hidden corrosion such as that occurring in lap splice joints [118]. Commercial systems capable of imaging corrosion damage have been developed and demonstrated [119]. Such systems possess millimeter-range resolution of localized corrosion cell processes.

SQUID magnetometers must be cooled to 77K in a liquid nitrogen dewar, which imposes a limit on how close the magnetometer can approach the sample. This imposes a significant constraint on system design because the ability to detect small flaws is dependent on the magnetometer coil size and the standoff. SQUID systems are good at scanning large surface areas quickly for evidence of corrosion, however, whether early stage corrosion defects can be detected with a high probability of observation remains to be established.

**7.3.2 Ultrasonic Methods.** Research in the area ultrasonic inspection is vigorous and has resulted in notable advances in recent years. Two example relevant to corrosion detection in dynamic system components include ultrasonic sensor array approaches have been developed to speed the rate of ultrasonic testing (UT) surveys [120, 121], and the emergence of guided wave UT techniques have been reported to detect corrosion thickness losses of 0.02 to 0.4mm [122], which is in the size range of interest for detection of early-stage corrosion.

**7.3.3 Pulsed Eddy Current Methods.** A problem with eddy current methods is the inability to distinguish crack-like flaws from artifacts, although the use of small “spot” probes and dual frequency [123] are examples of approaches that appear to provide greater sensitivity [124]. Advanced signal processing methods have been employed in conjunction with artificial neural network modeling to improve recognition of defect in eddy current signals [125].

**7.3.4 Integration and Fusion of NDE data.** Current thrusts in non-destructive evaluation include the integration of data collected from a range of techniques into a seamless assessment of a damaged structures [126], direct application of multi-source NDE data directly to an evaluation of component or structure reliability [127], or manufacturing process management [120] and signal processing and pattern recognition approaches for enhancing small signal detection to enhance the reliability of NDE measurements themselves and to increase probability of flaw detection [128, 129].

Development of suitable standard “flaws” for calibrating emerging NDE techniques continues to be an area of active research [130]. This is driven by the fact that there are essential elements of small defects produced by environmental effects that are not well simulated by artificially created defects. Additionally, there is difficulty in controlling laboratory-based damage mechanisms to replicate the size and morphology of in-service defects on an on-demand basis.

***Research recommendation.*** *To enhance safety and to enable the possibility of the of damage tolerance life-cycle management in dynamic systems, the probability of observation of discrete corrosion-induced defects of 0.5 mm and smaller must improve significantly. It is recommended that efforts be supported in this regard.*

## 8.0 REFERENCES

1. MIL-HDBK-1530, General Guidelines for Aircraft Structural Integrity Program 1996, Aeronautical Systems Center ASC/ENFS: Wright-Patterson AFB, OH.
2. R. A. Everett and W. Elber. Damage Tolerance Issues as Related to Metallic Rotorcraft Dynamic Components. in *Aging Systems: Application of Damage Tolerance Principles for Improved Airworthiness of Rotorcraft*. 1999. Corfu, Greece: NASA Center for AeroSpace Information (CASI).
3. S. C. Forth, D. Le, and J. Turnberg. An Evaluation of the Applicability of Damage Tolerance to Dynamic Systems. in *8th Joint NASA/FAA/DOD Aging Aircraft Conference*. 2005. Palm Springs, CA.
4. S. C. Forth, R. A. Everett, and J. A. Newman. A Novel Approach to Rotorcraft Damage Tolerance. in *6th Joint FAA/DOD/NASA Aging Aircraft Conference*. 2002.
5. D. Broek, *Elementary Fracture Mechanics*, 4th ed. 1986, Boston: Martinus Nijhoff Publishers. p. 282.
6. J. A. Harter, *AFGROW Users Guide and Technical Manual*. 1999, U.S. Air Force: WPAFB, OH.
7. S. R. Mettu, et al., *NASGRO 3.0: A Software for Analyzing Aging Aircraft*. 1999, NASA Center for AeroSpace Information (CASI).
8. R. P. Wei and D. G. Harlow, "Mechanistically-based Probability Modelling, Life Prediction and Reliability Assessment," *Modelling Simul. Mater. Sci. Eng.*, 13, R33-R51, (2005).
9. L. F. Mondolfo, *Aluminum Alloys: Structure and Properties*. 1976, Boston: Butterworths. p. 693.
10. K. S. Ferrer and R. G. Kelly, "Development of an aircraft lap joint simulant environment " *Corrosion*, 58, 452-459, (2002).
11. E. D. D. Doring, *Corrosion Atlas*, 3rd ed. 1997, New York: Elsevier. 578.
12. K. S. Lewis, R. G. Kelly, and R. S. Piascik. Determination of the Corrosive Conditions Present within Aircraft Lap-Splice Joints. in *The Second Joint NASA/FAA/DoD Conference on Aging Aircraft*. 1999.
13. N. Birbilis and R. G. Buchheit, "Electrochemical characteristics of intermetallic phases in aluminum alloys - An experimental survey and discussion " *J. Electrochem. Soc.*, 152, B140-B151, (2005).
14. R. R. Leard and R. G. Buchheit, "Electrochemical characterization of copper-bearing intermetallic compounds and localized corrosion of Al-Cu-Mg-Mn alloy 2024," *Materials Science Forum*, 396-4, 1491-1496, (2002).
15. R. G. Buchheit, "A compilation of Corrosion Potentials Reported for Intermetallic Phases in Aluminum Alloys," *J. Electrochem. Soc.*, 142, 3994-3996, (1995).
16. R. P. Wei, D. G. Harlow, and R. G. Buchheit, "work in progress," (2005).
17. N. R. Cawley and D. G. Harlow, "Spatial Statistics of Particles and Corrosion Pits in 2024-T3 Al Alloy," (1996).
18. R. G. Buchheit, J. P. Moran, and G. E. Stoner, "Localized Corrosion Behavior of Alloy 2090-The Role of Microstructural Heterogeneity," *Corrosion*, 46, 610-617, (1990).

19. T. J. R. Leclere and R. C. Newman, "Self-regulation of the cathodic reaction kinetics during corrosion of AlCu alloys " *J. Electrochem. Soc.*, B52-B56, (2002).
20. D. G. Harlow and R. P. Wei, "A Probability Model for the Growth of Corrosion Pits in Al Alloys Induced by Constituent Particles," *Eng. Fracture Mechanics*, 59, 305-525, (1998).
21. Z. Szklarska-Smialowska, Pit Initiation, in *Advances in Localized Corrosion*, U. B. H. Isaacs, J. Kruger, S. Smialowsak, eds., Editor. 1990, NACE, Houston, TX. p. 41-46.
22. G. S. Frankel, "Pitting Corrosion of Metals," *J. Electrochem. Soc.*, 145, 2186-2198, (1998).
23. D. E. Williams, C. Wescott, and M. Fleischmann, *J. Electrochem. Soc.*, 132, 1796, (1985).
24. D. E. Williams, J. Stewart, and P. H. Balkwill, *Corros. Sci.*, 36, 1213, (1994).
25. P. H. Balkwill, C. Wescott, and D. E. Williams, *Materials Science Forum*, 44&45, 299, (1989).
26. T. Shibata, *Corrosion*, 243, (1977).
27. J. Leifer and J. I. Mickalonis, "Prediction of aluminum pitting in natural waters via artificial neural network analysis," *Corrosion*, 56, 563-571, (2000).
28. R. P. Wei, C.-M. Liao, and M. Gao, "A Transmission Electron Microscopy Study of Constituent-Particle-Induced Corrosion in 7075-T6 and 2024-T3 Al Alloys," *Metall. Trans. A*, 29A, 1153-1160, (1998).
29. R. P. Wei, "A Model for Particle -Induced Pit Growth in Al Alloys," *Scripta Mater.*, 44, 2647-2652, (2001).
30. E. D. D. Doring, *Corrosion Atlas*, 3rd ed. 1997, New York: Elsevier. 597.
31. R. G. Buchheit, et al., "Local Dissolution Phenomena Associated with S Phase (Al<sub>2</sub>CuMg) in Al-Cu-Mg Alloys," *J. Electrochem. Soc.*, 144, 2621-2628, (1997).
32. D. G. Harlow and R. P. Wei, "Probability Modeling and Statistical Analysis of Damage in the Lower Wing Skins of Two Retired B-707 Aircraft," *Fatigue & Fracture of Engineering Materials & Structures*, 24, 523-535, (2001).
33. A. Garner and D. Tromans, "Direct Observation of Intergranular Corrosion in Al-4wt%Cu Alloy," *Corrosion*, 35, 55-60, (1979).
34. I. L. Muller and J. R. Galvele, *Corros. Sci.*, 17, 179, (1977).
35. M. S. Hunter, G. R. Frank, and D. L. Robinson, *Mechanism of Corrosion of 2024 Aluminum Alloy as Revealed by Electron Microscopy*. 1963, Aluminum Company of America: New Kensington, PA.
36. H. Nichols and W. Rostoker, "Intergranular Corrosion Penetration in an Age-Hardenable Aluminum Alloy," *J. Electrochem. Soc.*, 112, 108-109, (1965).
37. W. L. Zhang and G. S. Frankel, "Localized corrosion growth kinetics in AA2024 alloys," *Journal of the Electrochemical Society*, 149, B510-B519, (2002).
38. X. D. Liu, et al., "Effect of applied tensile stress on intergranular corrosion of AA2024-T3," *Corrosion Science*, 46, 405-425, (2004).
39. S. L. Ruan, et al., "Statistical modeling of minimum intergranular corrosion path length in high-strength aluminum alloy," *Technometrics*, 46, 69-75, (2004).

40. S. L. Ruan, D. A. Wolfe, and G. S. Frankel, "Statistical modeling and computer simulation of intergranular corrosion growth in AA2024-T3 aluminum alloy," *Journal of Statistical Planning and Inference*, 126, 553-568, (2004).
41. D. McNaughtan, M. Worsfold, and M. J. Robinson, "Corrosion product force measurements in the study of exfoliation and stress corrosion cracking in high strength aluminium alloys," *Corrosion Science*, 45, 2377-2389, (2003).
42. M. J. Robinson, "The Role of Wedging Stresses in the Exfoliation Corrosion of High-Strength Aluminum-Alloys," *Corrosion Science*, 23, 887-&, (1983).
43. M. J. Robinson and N. C. Jackson, "Exfoliation corrosion of high strength Al-Cu-Mg alloys: effect of grain structure," *British Corrosion Journal*, 34, 45-49, (1999).
44. M. J. Robinson, "Mathematical-Modeling of Exfoliation Corrosion in High-Strength Aluminum-Alloys," *Corrosion Science*, 22, 775-&, (1982).
45. T. Y. Liu, J. S. Robinson, and M. A. McCarthy, "The influence of processing and microstructural parameters on the exfoliation corrosion susceptibility of 2025, in Aluminum Alloys 2002: Their Physical and Mechanical Properties Pts 1-3. 2002. p. 1419-1424.
46. T. Y. Liu, J. S. Robinson, and M. A. McCarthy, "The influence of hot deformation on the exfoliation corrosion behaviour of aluminium alloy 2025," *Journal of Materials Processing Technology*, 153-54, 185-192, (2004).
47. W. L. Zhang and G. S. Frankel, "Transitions between pitting and intergranular corrosion in AA2024," *Electrochimica Acta*, 48, 1193-1210, (2003).
48. E. A. G. Liddiard, J. A. Whittaker, and H. K. Farmery, "The Exfoliation Corrosion of Aluminum Alloys," *J. Inst. Metals*, 89, 377, (1960).
49. X. Zhao, et al., "In situ X-ray radiographic study of intergranular corrosion in aluminum alloys," *Corrosion*, 59, 1012-1018, (2003).
50. T. D. Burleigh, "The Postulated Mechanisms for Stress Corrosion Cracking of Aluminum Alloys: A Review of the Literature 1980-1989," *Corrosion*, 47, 89-98, (1991).
51. M. O. Speidel, "Stress Corrosion Cracking of Aluminum Alloys," *Metall. Trans. A*, 6, 631-651, (1975).
52. R. C. Newman and R. P. M. Procter, "Stress Corrosion Cracking: 1965-1990," *British Corrosion Journal*, 25, 259-269, (1990).
53. C. E. Harris, et al., "Analytical Methodology for Predicting Widespread Fatigue Damage Onset in Fuselage Structure," *J. of Aircraft*, 35, 307-317, (1998).
54. D. Y. Jeong and P. Tong, "Onset of Multiple Site Damage and Widespread Fatigue," *International Journal of Fatigue*, 85, 185-200, (1997).
55. R. Jones, et al., "Developments in the Analysis of Interacting Cracks," *Engineering Failure Analysis*, 2, 307-320, (1995).
56. S. Pitt and R. Jones, "Multiple-Site and Widespread Fatigue Damage in Aging Aircraft," *Engineering Failure Analysis*, 4, 237-257, (1997).
57. P. Shi and S. Mahadevan, "Damage Tolerance Approach for Probabilistic Pitting Corrosion Fatigue Life Prediction," *Engineering Fracture Mechanics*, 68, 1493-1507, (2001).
58. K. K. Sankaran, R. Perez, and K. V. Jata, "Effects of Pitting Corrosion on the Fatigue Behavior of Aluminum Alloy 7075-T6: Modeling and Experimental Studies," *Materials Sci. & Eng. A*, A297, 223-229, (2001).

59. Standard Practice for Modified Salt Spray (Fog) Testing, in Annual Book of ASTM Standards, Section 3, Wear Erosion; Metal Corrosion, E. R. F. Allen, Editor. 1999, ASTM: West Conshohocken, PA. p. 367.
60. G. S. Chen, et al., "Transition from Pitting to Fatigue Crack Growth -Modeling of Corrosion Fatigue Crack Nucleation in a 2024-T3 Al Alloy," *Materials Sci. & Eng. A*, A219, 126-132, (1996).
61. D. G. Harlow and R. P. Wei, "Probability Approach for Prediction of Corrosion and Corrosion Fatigue Life," *AIAA Journal*, 32, 2073-2079, (1994).
62. R. G. Buchheit and A. E. Hughes, Chromate and Chromate-Free Conversion Coatings, in *Metals Handbook Vol. 13A*, S. D. Cramer and B. S. Covino, Editors. 2003, ASM International. p. 720.
63. M. W. Kendig and R. G. Buchheit, "Corrosion Inhibition of Al and Al Alloys by Hexavalent Cr Compounds," *Corrosion*, 59, 379-400, (2003).
64. K. Ogle and R. G. Buchheit, Conversion Coatings, in *Encyclopedia of Electrochemistry*, edited by , Vol. 4, Corrosion and Oxide Films, A. J. Bard and M. Stratmann, Editors. 2003, Wiley-VCH: Weinheim, Germany. p. 460-499.
65. L. Xia and R. L. McCreery, *J. Electrochem. Soc.*, 145, 3083, (1998).
66. S. M. Cohen, *Corrosion*, 51, 71, (1995).
67. B. W. R. Hinton, *Metal Finishing*, 89, 55, (1991).
68. B. W. R. Hinton, *Metal Finishing*, 89, 15, (1991).
69. R. L. Twite and G. P. Bierwagen, *Prog. Org. Coat.*, 33, 91, (1998).
70. F. Report, Alternatives to Chromium for Metal Finishing. 1995, National Center for Manufacturing Sciences: Ann Arbor, MI.
71. J. T. Report, Validation of Alternatives to Chromate Conversion Coatings for Aluminum Alloys 2024, 6061, 7075 and Ion Vapor Deposited Aluminum on Steel. 1997, NDCEE/CTC: Johnstown, PA.
72. J. T. Report, Laboratory Validation (Testing) of Alternatives to Chromate-Containing Primer Coatings for Aircraft Exterior Mold-Line Skins. 1998, NDCEE/CTC: Johnstown, PA.
73. J. T. Report, Validation of Low/No VOC and Non-Chromate Coating Systems for Support Equipment. 2001, NDCEE, CTC: Johnstown, PA.
74. R. G. Buchheit, et al., *Corrosion*, 58, 3, (2002).
75. W. van Ooij and D. Zhu, "Electrochemical impedance spectroscopy of bis-[triethoxysilylpropyl]tetrasulfide on Al 2024-T3," *Corrosion*, 57, 413-427, (2001).
76. W. vanOoij, et al., "Silane based chromate replacements for corrosion control, paint adhesion, and rubber bonding," *Surf. Eng.*, 16, 386-396, (2000).
77. J. H. Osborne, et al., "Testing and evaluation of nonchromated coating systems for aerospace applications," *Prog. Org. Coatings*, 41, 217-225, (2001).
78. J. H. Osborne, et al., *Advanced Corrosion Resistant Aircraft Coatings*. 2000, Air Force Materiel Command: Wright-Patterson AFB, OH.
79. R. L. Cook and S. R. Taylor, *Corrosion*, 56, 321, (2000).
80. *Recent Alternatives to Chromate for Aluminum Conversion Coating*. 2002, National Center for Manufacturing Sciences, Inc.: Ann Arbor, MI.
81. T. V. Philip, Ultrahigh-Strength Steels, in *Metals Handbook*, 9th Ed. , B. P. Bardes, Editor. 1978, ASM Metals Park, OH. p. p. 421-443.

82. A. Oehlert and A. Atrens, "The Initiation and Propagation of Stress Corrosion Cracking in AISI 4340 and 3.5 Ni-Cr-Mo-V Rotor Steel in Constant Load Tests," *Corros. Sci.*, 38, 1159-1169, (1996).
83. T. L. Chang, L. W. Tsay, and C. Chen, "Influence of gaseous Hydrogen on the Notched Tensile Strength of D6ac Steel," *Materials Sci. & Engg. A*, A316, 153-160, (2001).
84. J. Y. Mann and D. S. Kemsley, *Corrosion*, 35, 465, (1979).
85. D. J. M. Jr. and G. W. Geil, Pitting and Its Effect on the Fatigue Limit of Steels Corroded Under Various Conditions, in *Proceedings of ASTM*. 1941. p. 696-732.
86. Z. Szklarska-Smialowska, *Pitting Corrosion of Metals*. 1986, Houston, TX: NACE.
87. Y. Kondo, "Prediction of Fatigue Crack Initiation Life Based on Pit Growth," *Corrosion*, 45, 7-11, (1989).
88. M. Nakajima and K. Tokaji, "Fatigue Life Distribution and Growth of Corrosion Pits in a Medium Carbon Steel in 3% NaCl Solution," *Fatigue Fract. Engng. Mater. Struct.*, 18, 345-351, (1995).
89. S. Zhou and A. Turnbull, "Development of Pre-pitting Procedure for Turbine Disc Steel," *British Corrosion Journal*, 35, 120-124, (2000).
90. A. Turnbull, L. N. McCartney, and S. Zhou. A Deterministic Model of Pitting Corrosion and the Pit-to-Crack Transition. in *Proceedings of EICM-2*. September, 2004. Banff, Canada.
91. T. Shibata and T. Takeyama, *Corrosion*, 33, 243, (1977).
92. N. Eliaz, et al., "Characteristics of Hydrogen Embrittlement, Stress Corrosion Cracking and Tempered Martensite Embrittlement in High Strength Steels," *Engineering Failure Analysis*, 9, 167-184, (2002).
93. G. E. Kerns, M. T. Wang, and R. W. Staehle. *Stress Corrosion Cracking and Hydrogen Embrittlement in High Strength Steels*. in *Stress Corrosion Cracking and Hydrogen Embrittlement in Iron-Base Alloys*. 1973. Unieux-Firminy, France: NACE.
94. D. A. Vermilyea. *Reaction Films, Metal Dissolution and Stress Corrosion Cracking*. in *Fundamental Aspects of Stress Corrosion Cracking*. 1967. Columbus, OH: NACE.
95. L. J. Korb, *Corrosion in the Aerospace Industry*, in *Metals Handbook*, 9th ed. , L. J. Korb and D. L. Olson, Editors. 1987, ASM. p. 1087.
96. T. C. Lindley, P. McIntyre, and P. J. Trant, "Fatigue-Crack Initiation at Corrosion Pits," *Metals Technology*, 9, 135-142, (1982).
97. T. Sydberger, *Werkstoffe und Korrosion*, 32, 119, (1981).
98. M. A. Streicher, *J. Electrochem. Soc.*, 103, 375, (1956).
99. R. M Hudson, R. J. Joniec, and S. R. Shatynski, *Pickling of Iron and Steel*, in *Metals Handbook Vol. 5*. 1987, ASM International: Materials Park, OH.
100. B. Gaur, T. B. Singh, and D. D. N. Singh, *Corrosion*, 52, 154, (1996).
101. E. E. H. Phelps, in *The Making Shaping and Treating of Steel*. 1971, U.S. Steel Corp.: Pittsburgh, PA. p. 802.
102. A. H. Tuthill, *Advance Materials and Processes*, 34, (1992).
103. J. Pilznienski, *Acid Cleaning of Iron and Steel*, in *Metals Handbook Vol. 5*. 1987, ASM International: Materials Park, OH.

104. K. Legg, Cadmium Replacement Alternatives for the Joint Strike Fighter. 2000, Rowan Technology Group: Libertyville, IL.
105. M. Bielawski, "Development of UNbalanced Magnetron Sputtered Al-Mo Coatings for Cadmium Replacement," *Surface Coatings and Tecnology*, 179, 10-17, (2004).
106. J. Mazia and D. Lashmore, Electroplated Coatings, in *Metals Handbook*, 9th ed., L. J. Korb and D. L. Olson, Editors. 1987, ASM: Metals Park, OH. p. 419.
107. M. P. Nascimento, et al., "Effects of Tungsten Crbide Thermal Spray Coating by HP/HVOF and Hard Chromium Electroplating on AISI 4340 High Strength Steel," *Surface Coatings and Tecnology*, 138, 113-124, (2001).
108. H. J. C. Voorwald, et al., "Evaluation of WC-17Co and WC-10Co-4Cr Thermal Spray Coatings by HVOF on the Fatigue and Corrosion Strength of 4340 Steel," *Surface Coatings and Tecnology*, 190, 155-164, (2005).
109. C. V. Franco, et al., "An Electrochemical Study of Magnetron-Sputtered Ti- and TiN-Coated Steel," *Corros. Sci.*, 40, 103-112, (1998).
110. F. Oleveira, et al., "Corrosion-Fatigue properties of a 4340 Steel Coated ith Colmonoy 88 Alloy, Applied by HVOF Thermal Spray," *Surface Coatings and Tecnology*, 140, 128-135, (2001).
111. T. Segawa, H. Sasahara, and M. Tsutsumi, "Development of a New Tool to Generate Compressive Residual Stress Within a Machined Surface," *Machine Tools and Manufacture*, 44, 1215-1221, (2004).
112. C. D. Smith, Federal Aviation Administration Aircraft Inspection Research and Development Programs, in *Nondestructive Evaluation of Aging Aircraft, Airports, and Aerospace Hardware*, R. D. Rempt and A. L. Broz, Editors. 1996, Proc. SPIE 2945. p. 200-209.
113. R. Halmshaw, *Non-Destructive Testing*. 1987, London: Edward Arnold. 109.
114. B. Zoofan, et al., "Application of Phase Contrast Microradiography in NDT," *Materials Evaluation*, 63, 1122-1127, (2005).
115. H. Weinstock, "A Review of SQUID Magnetometry Applied to Non-Destructive Evaluation," *IEEE Transactions on Magnetics*, 27, 3231-3236, (1991).
116. R. Hohmann, et al., "HTS SQUID System with Joule-Thompson Cryocooler for Eddy Current Nondestructive Evaluation of Aircraft Structures," *IEEE Transactions on Applied Superconductivity*, 7, 2860-2865, (1997).
117. E. Juzeliunas and J. H. Hinken, "Corrosion Sensing by SQUID Magnetometry," *J. Electronanal. Chem.*, 477, 171-177, (1999).
118. A. Abedi, et al., "A Superconducting Quantum Interference Device Magnetometer System for Quantitative Analysis and Imaging of Hidden Corrosion Activity in Aircraft Aluminum Structures," *Review of Scientific Instruments*, 70, 4640-4651, (1999).
119. Y. P. Ma, et al., "Magnetic Fields Induced by Electrochemical Reactions: Aluminum Alloy Corrosion Sensing by SQUID Magnetometry on a Macroscopic Scale," *J. Phys. Chem.*, 106, 12549-12555, (2002).
120. M. Jagd, K. W. Nielsen, and J. Rheinlander, "Non-Destructive Evaluation to Control New Casting Processes," *Insight*, 45, 134-136, (2003).
121. S. J. Willsher and R. A. Smith, "Multi-element Ultrasonic Scanning of In-service Airframes," *Insight*, 40, 154-159, (1998).

122. W. Zhu, et al., "Ultrasonic Guided wave NDT for Hidden Corrosion Detection," *Research in NDE*, 10, 205-225, (1998).
123. B. Sasi, B. P. C. Rao, and T. Jayakumar, "Dual-Frequency Eddy Current Non-Destructive Detection of Fatigue Cracks in Compressor Disks or Aero Engines," *Defence Science Journal*, 563-570, (2004).
124. S. R. Kramer and J. F. Harmon, "Eddy Current Testing to Detect Cracks and Corrosion in the P-3C Orion Vertical Stabilizer Spar Caps," *Materials Evaluation*, 59, 166-169, (2001).
125. M. C. Petri, et al., "Eddy Current Signal Deconvolution Technique for the Improvement of Steam Generator Tubing Burst Pressure Predictions," *J. Nondestructive Eval.*, 19, 149-164, (2000).
126. L. K. Shark, B. J. Matuszewski, and J. P. Smith, "Automatic Feature-based Fusion of Ultrasonic, Radiographic and Shearographic Images for Aerospace NDT," *Insight*, 43, 607-615, (2001).
127. E. B. Shell, R. G. Buchheit, and B. Zoofan, "Correlation of Residual Fatigue Strength with quantified NDE Measurements," *International Journal of Fatigue*, 27, 105-112, (2005).
128. D. V. Leemans and D. Forsyth, "Bayesian Approaches to Using Field Test Data in Determining the Probability of Detection," *Materials Evaluation*, 62, 855-859, (2004).
129. N. Yusa, Z. M. Chen, and K. Miya, "Rapid REconstruction of Natural Stress Corrosion Cracking From Eddy Current NDT Data," *Key Engineering Materials*, 270-273, 593-599, (2004).
130. M. Kemppainen, et al., "Advanced Flaw Production Method for In-service Inspection Qualification Mock-ups," *Nuclear Engineering and Design*, 224, 105-117, (2003).